Different Mars-solar wind interaction models: implications for ENA imaging

H. Gunell,* M. Holmström, and S. Barabash
Swedish Institute of Space Physics, Kiruna, Sweden

E. Kallio and P. Janhunen
Finnish Meteorological Institute, Helsinki, Finland

A. F. Nagy and Y. Ma
University of Michigan, Ann Arbor, Michigan, USA

Introduction

Three different models of the interaction between the solar wind and Mars have been examined here, with emphasis on the generation of ENA images. The three models are:

1. an empirical model that is based on Phobos 2 measurements [1],
2. a 3D MHD simulation [2], and
3. a 3D hybrid simulation [3, 4].

Hydrogen ENA images from the empirical model were computed and published by Holmström, et al., [5]. They calculated the ENA emission by combining the empirical model of the plasma flow with a model for the neutral gas density of the Martian atmosphere, using cross sections for the relevant charge exchange reactions. The ENA images are then generated by integrating the ENA emission along lines of sight to a virtual ENA instrument. A similar approach was used by Barabash, et al., [6] to generate oxygen ENA images; the difference being that the flow of oxygen ions was given by a test particle simulation, where trajectories of oxygen ion test particles moving in the electric and magnetic fields of the empirical model were calculated.

ENA images from the MHD model are generated in the same way as with the empirical model. The flows of hydrogen and oxygen ions are given by the output of the MHD code and these are combined with the models of the neutral gas densities and cross sections. Fig. 1 shows an example of the plasma flow, and Fig. 2 shows the neutral gas density as a function of altitude.

The hybrid code is able to generate its own discrete ENAs since the position and velocity of all super-ions are known at each time step. The probability for an ion to have a charge exchange collision is then found from the neutral density and the energy dependent cross section. The weight of the super-ion is reduced in proportion to the probability of a charge exchange collision. Charge exchange collisions are thus accounted for self-consistently. The super-ion velocities, positions, and weights are saved periodically, and the images are generated when the simulation has been run by computing the trajectories of the super-ENAs and collecting them with a virtual ENA instrument.

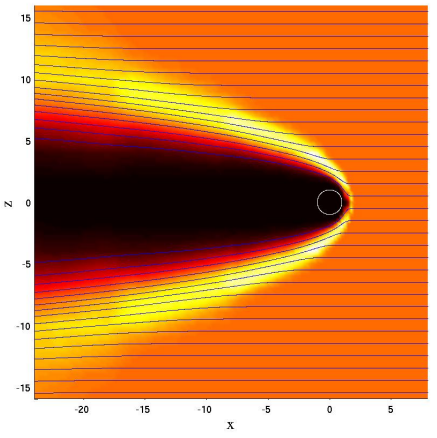

FIG. 1: Plasma flow in the MHD model.

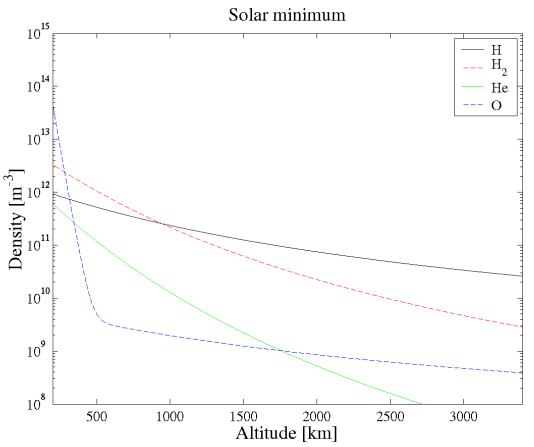

FIG. 2: Neutral gas densities.

*Electronic address: herbert.gunell@physics.org; URL: http://www.irf.se/~herbert

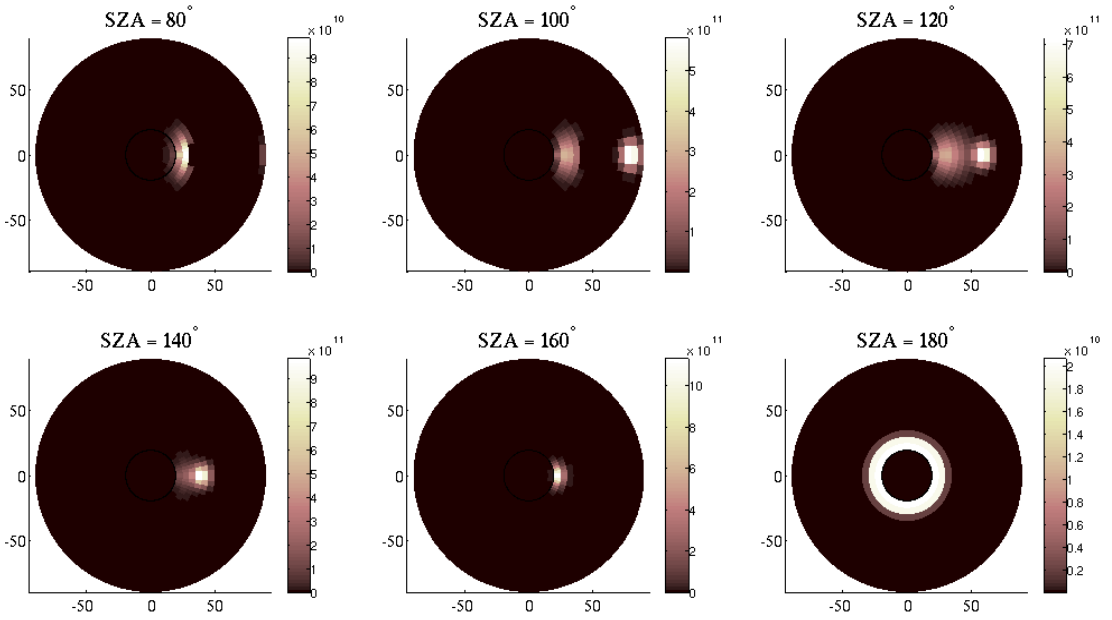

FIG. 3: Hydrogen ENA-images from the empirical model. The solar zenith angles are 80°, 100°, 120°, 140°, 160°, and 180°. The ENA flux is shown in units of $\mathrm{sr}^{-1}\mathrm{m}^{-2}\mathrm{s}^{-1}$.

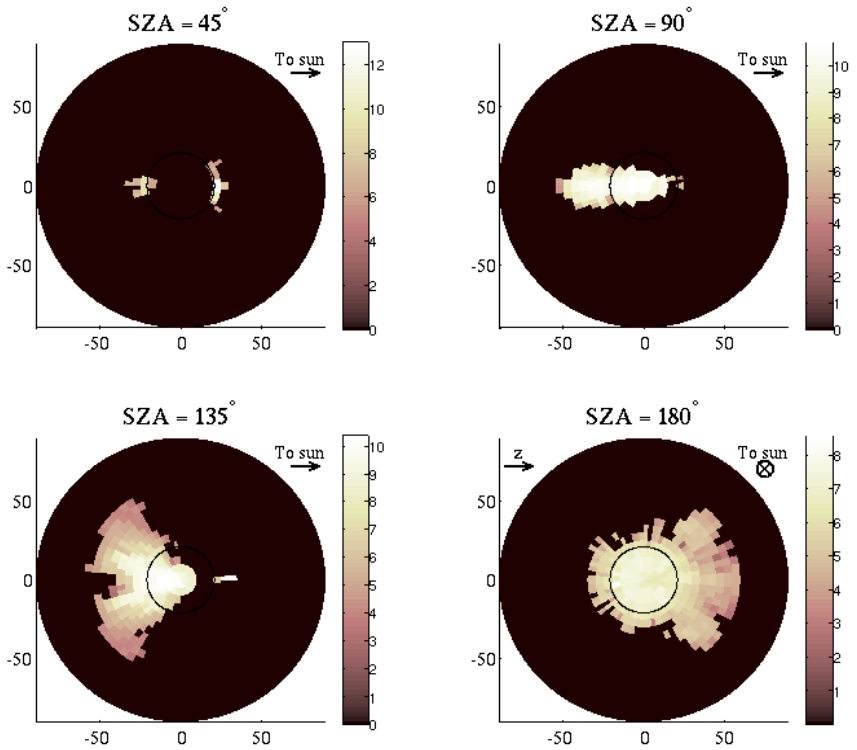

FIG. 4: Oxygen ENA-images from the empirical model. The solar zenith angles are 45°, 90°, 135°, and 180°. The ENA flux is shown in units of $\mathrm{sr}^{-1}\mathrm{m}^{-2}\mathrm{s}^{-1}$.

The empirical model

Fig. 3 shows hydrogen ENA images from vantage points in the $x-z$-plane, three Mars radii away from the centre of Mars. The structure and shape of the images are in reasonable agreement with the MHD model (next page), although the absolute values of the ENA flux are slightly lower in the images produced by the empirical model. There are two maxima in the ENA flux; one produced upstream in the solar wind and another closer to, but separated from, the planet.

Fig. 4 shows oxygen ENA images from vantage points in the $x-z$-plane, three Mars radii away from the centre of Mars.

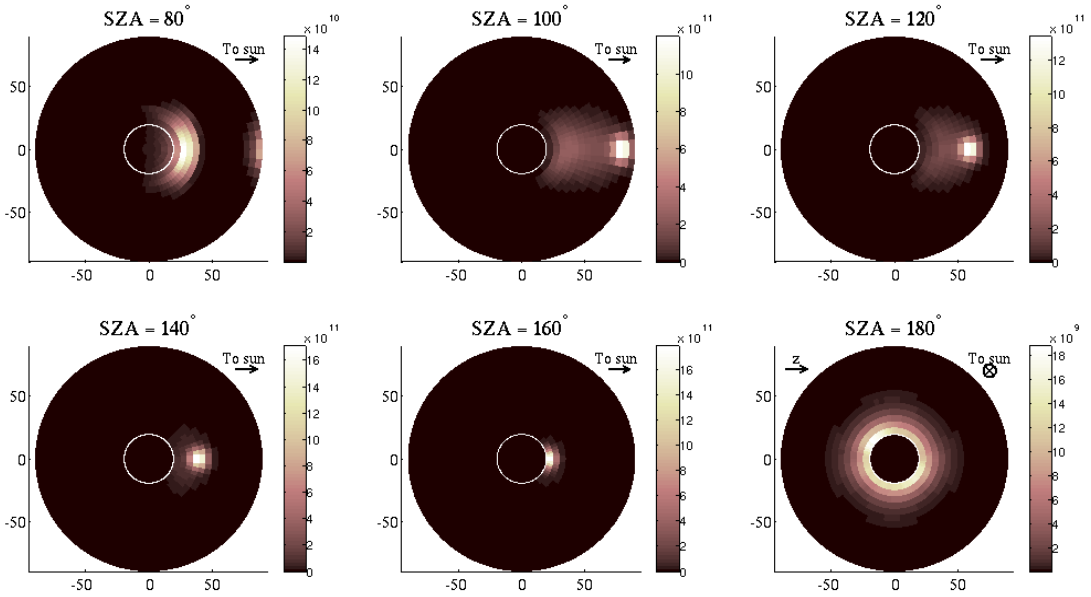

FIG. 5: The hydrogen ENA-images. The solar zenith angles are 80°, 100°, 120°, 140°, 160°, and 180°. The ENA flux is shown in units of $\mathrm{sr}^{-1}\mathrm{m}^{-2}\mathrm{s}^{-1}$.

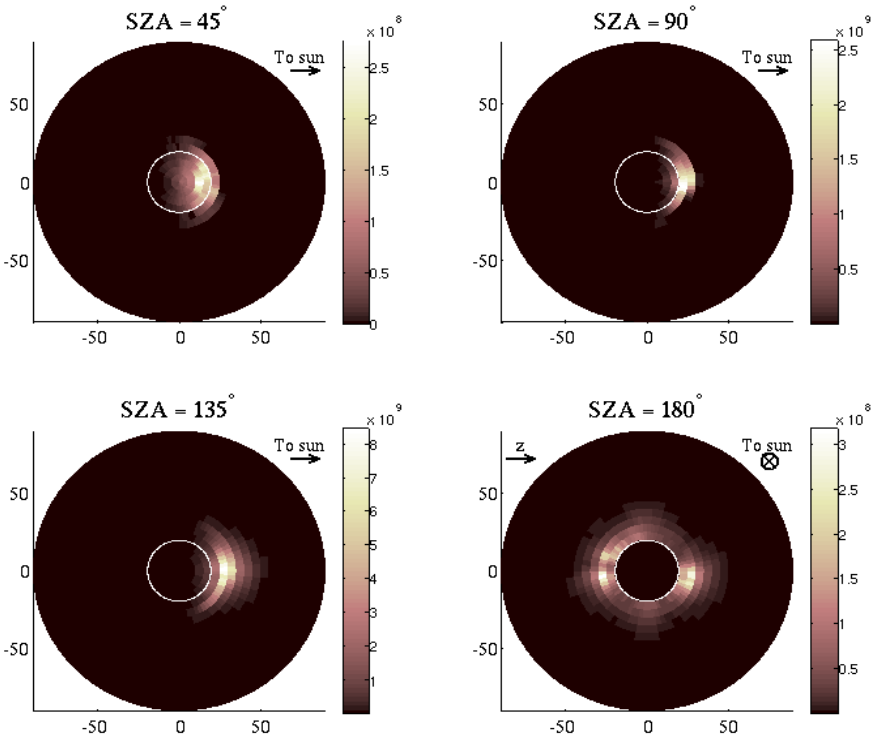

FIG. 6: The oxygen ENA-images. The solar zenith angles are 45°, 90°, 135°, and 180°. The ENA flux is shown in units of $\mathrm{sr}^{-1}\mathrm{m}^{-2}\mathrm{s}^{-1}$.

The MHD simulation

Fig. 5 shows hydrogen ENA images from vantage points in the $x-z$-plane, three Mars radii away from the centre of Mars. The maximum at the right hand side of the figure represents ENAs produced in the solar wind. There is also a local maximum close to, but separated from, the planet. As the vantage point is moved toward the nightside of Mars in the subsequent panels the maximum associated with ENAs produced upstream in the solar wind moves toward the centre of the image and is dominating over the other maximum. Fig. 6 shows oxygen ENA images from vantage points in the $x-z$-plane, three Mars radii away from the centre of Mars.

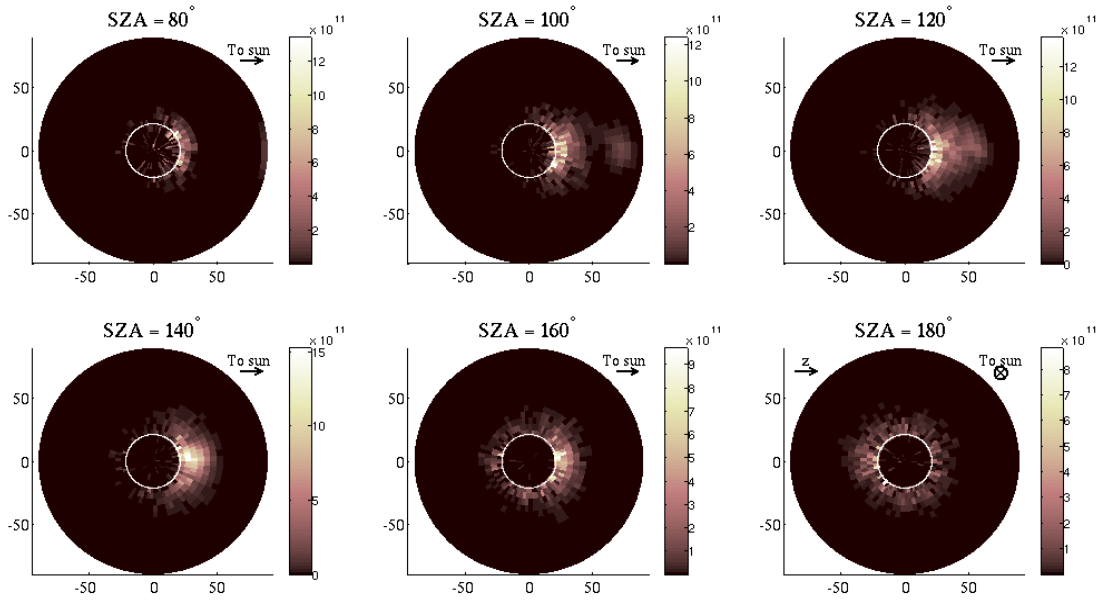

FIG. 7: Hydrogen ENA-images produced by the hybrid model. Mars is viewed from a vantage point three Martian radii from the centre of Mars. From left to right, starting at the upper left panel, the solar zenith angles of the vantage points are $80°, 100°, 120°, 140°, 160°$, and $180°$. The ENA flux is shown in units of $\mathrm{sr}^{-1}\mathrm{m}^{-2}\mathrm{s}^{-1}$.

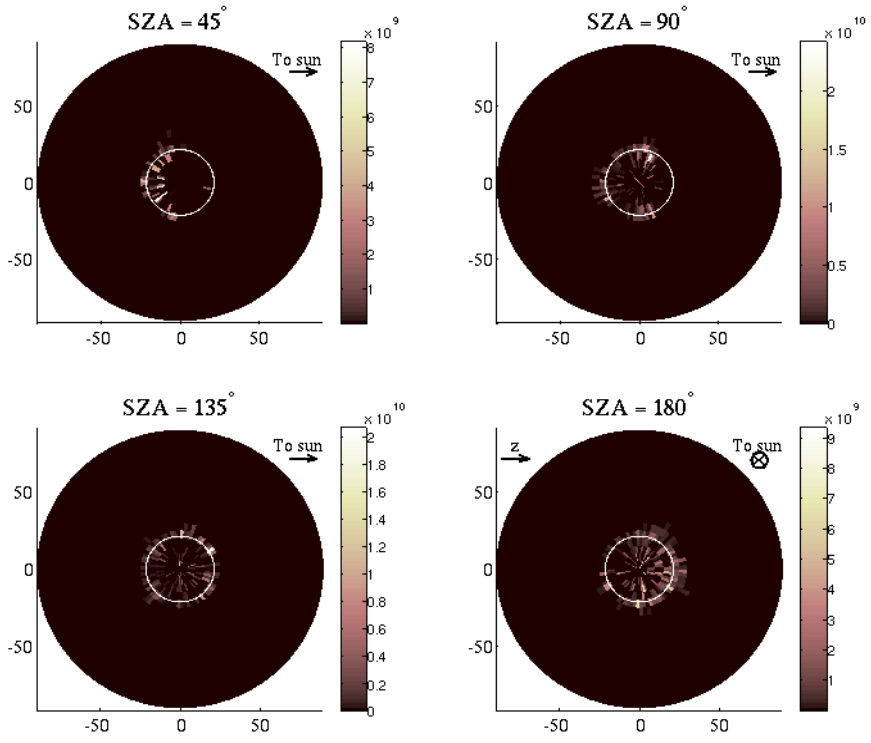

FIG. 8: Same as Fig. 7, but for oxygen ENAs.

The hybrid simulation

Hydrogen ENA images generated from the same vantage points as the images published by Holmström, et al., [5] are shown in Fig. 7. Fig. 8 shows oxygen ENA images.

A local maximum on the right hand side of the pictures representing ENAs produced upstream in the solar wind can be seen (although it is faint). The other (main) maximum is not separated from the planet, which means that this model does not produce any "protonopause".

The asymmetry in the oxygen images is a result of the asymmetry in the O^+ density.

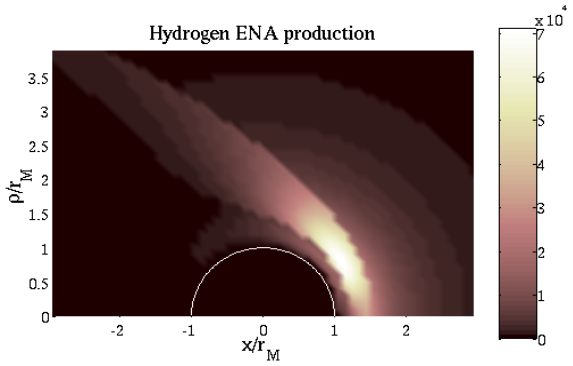

FIG. 9: Production of hydrogen ENAs in the empirical model. The production rate is given in units of $\mathrm{m}^{-3}\mathrm{s}^{-1}$. The cylindrical coordinate $\rho = \sqrt{y^2 + z^2}$ is the distance from the Mars–sun line.

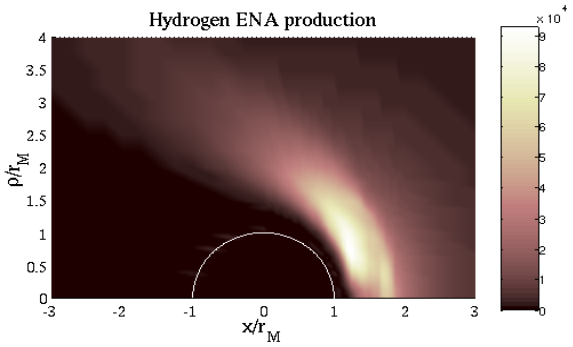

FIG. 10: Production of hydrogen ENAs in the MHD model.

ENA production

The production rate for hydrogen ENAs is shown in Fig. 9 for the empirical model, in Fig. 10 for the MHD model and in Fig. 11 for the hybrid model. The production rates have been integrated over the azimuthal coordinate.

In the empirical model the maximum is located about one Mars radius off the x-axis, and the ENA production on the x-axis above noon is small.

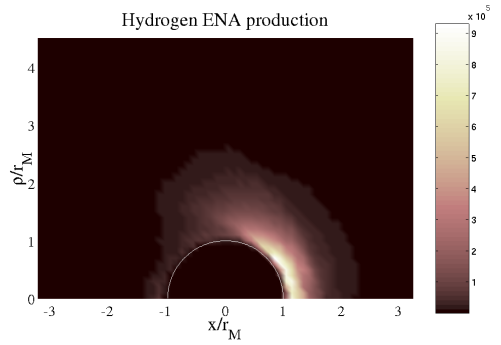

FIG. 11: Hydrogen ENA production (hybrid model).

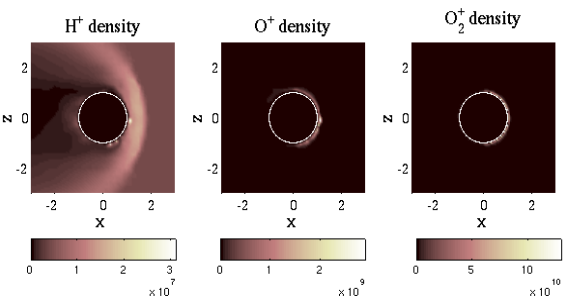

FIG. 12: Density of the ion species (MHD model).

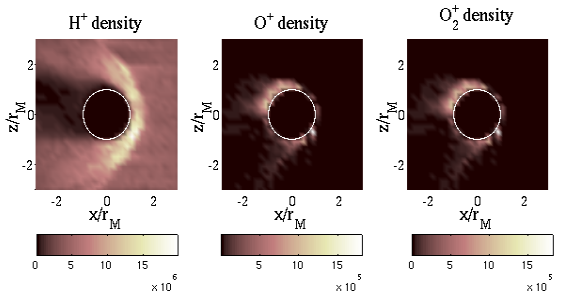

FIG. 13: Ion densities (hybrid model).

In the MHD model (Fig. 10) the global maximum is located off the Mars-sun line like it is in the empirical model, however a significant production rate is found on the Mars-sun line like it is in the hybrid model. The region with a high ENA production rate is located further away from the planet in the MHD model than in the other models.

In the hybrid simulation considered here the maximal production rate appears close to the planet about half a Mars radius away from the x-axis on the sunny side of Mars. Outside the global maximum there is a region of significant ENA production extending down to the x-axis.

Density

In Fig. 12 the density of the three ion species in the $x - z$-plane is shown. Fig. 13 shows the same thing for the hybrid model. The MHD model resolves much higher densities of O^+ and O_2^+ close to the planet than the hybrid model.

It is seen from Fig. 13 that there is a north–south asymmetry in the density in the hybrid model. The ion density near Mars depends on $\vec{E}\times\vec{B}$-drifts and on emission of ionospheric ions. To properly account for the boundary conditions at the ionosphere is thus important for a correct modelling of the density distribution.

Summary and conclusions

- We have simulated ENA images based on three different models of the plasma flow around Mars.
- The hybrid model does not produce a "magnetopause", when run with the present parameters and a grid size of 720 km$\approx$ $0.2R_M$, and thus ENAs are produced all the way down to the obstacle boundary. In the MHD model on the other hand the production region is clearly separated from the planet.
- The maximum of the ENA production rate is located away from the Mars–sun line in all models, however, in the hybrid and MHD models there is a region of significant ENA production extending down to the Mars–sun line. The MHD model even shows two separated local maxima; one on the Mars–sun line and one away from it.
- To make accurate predictions by the use of computer models knowledge of the boundary conditions is required.
- In the hybrid simulation the O^+ density distribution develops an asymmetry, which shows up in the oxygen ENA images. This suggests that ENA images can serve as remote measurements of the O^+ density distribution.
- Finally the opinion of the first author: MHD simulations probably are the best self consistent models of the Mars-solar wind interaction available at this time, but hybrid codes are likely to win in the future when the available computer capacity increases. Future development of new models will have to include kinetic phenomena and the coupling between phenomena occurring on small and large scales. Clever new approaches in particle simulations will be required, and care must be taken to properly include boundary conditions, which will require more measurements by space-craft carried instruments.

---

[1] E. Kallio, J. G. Luhmann, and S. Barabash, "Charge exchange near Mars: The solar wind absorption and energetic neutral atom production," *Journal of Geophysical Research*, vol. 102, pp. 22183–22197, 1997.

[2] Y. Ma, A. F. Nagy, K. C. Hansen, D. L. DeZeeuw, and T. I. Gombosi, "Three-dimensional multispecies MHD studies of the solar wind interaction with Mars in the presence of crustal fields," *Journal of Geophysical Research*, vol. 107, 09 October 2002. 10.1029/2002JA0092935.

[3] E. Kallio and P. Janhunen, "Atmospheric effects of proton precipitaion in the Martian atmosphere and its connection to the Mars-solar wind interaction," *Journal of Geophysical Research*, vol. 106, pp. 5617–5634, 2001.

[4] E. Kallio and P. Janhunen, "Ion escape from Mars in a quasi-neutral hybrid model," *Journal of Geophysical Research*, vol. 107, 19 March 2002. 10.1029/2001JA000090.

[5] M. Holmström, S. Barabash, and E. Kallio, "Energetic neutral atoms at Mars I: Imaging of solar wind protons," *Journal of Geophysical Research*, vol. 107, 09 October 2002. 10.1029/2001JA000325.

[6] S. Barabash, M. Holmström, A. Lukyanov, and E. Kallio, "Energetic neutral atoms at Mars IV: Imaging of planetary oxygen," *Journal of Geophysical Research*, vol. 107, 09 October 2002. 10.1029/2001JA000326.